Inorg. Chem. **2008**, *47*, 10959−10964

Room Temperature Antiferromagnetic Order in the Mn(II) Oxide 4H-$Ba_{0.5}Sr_{0.5}MnO_{2+\delta}$

Josephine J. Adkin and Michael A. Hayward*

Department of Chemistry, Inorganic Chemistry Laboratory, University of Oxford, South Parks Road, Oxford OX1 3QR, United Kingdom

Received June 26, 2008

The synthesis of the Mn(II) phase 4H-$Ba_{0.5}Sr_{0.5}MnO_{2+\delta}$ via the topotactic reduction of 4H-$Ba_{0.5}Sr_{0.5}MnO_{3-x}$ with the novel reducing agent LiH, is described. Neutron powder diffraction data show that oxide ions are deintercalated from the host structure in a disordered manner to yield "tetrahedral" MnO_4 coordination sites. Magnetic susceptibility and neutron powder diffraction data show that the title phase adopts a canted antiferromagnetically ordered state below $T_N = 355$K, consistent with the strong magnetic coupling expected between d^5 centers.

Introduction

Complex transition metal oxides have been the subject of extensive and enduring study because of the wide range of physical properties they exhibit. Particular interest has focused on materials based on ABO_3 (A = Group 1, 2 or Lanthanide; B = transition metal) perovskite compositions because of the observation of strong coupling between the electronic states of neighboring transition metal centers.[1] The structures adopted by ABO_3 phases can be rationalized by the structural tolerance factor, t ($t = \langle A-O\rangle/\sqrt{2}\langle B-O\rangle$).[2] Compositions with tolerance factors equal to unity have the geometrically ideal ratio of A−O and B−O bond lengths to adopt the cubic perovskite structure in which AO_3 layers are stacked in a cubic ABCABC manner and the B cations occupy sites between these layers to form a three dimensional network of corner sharing BO_6 octahedra. Small deviations of the tolerance factor below unity are accommodated by cooperative twisting and tilting distortions of the BO_6 octahedra in which the B−O−B bond angle is reduced below 180° to accommodate small A-site cations. If the tolerance factor takes values greater than unity, hexagonal ABAB stacking of the AO_3 layers is introduced into the structure to expand the A-cation sites. This leads to the introduction of face-shared links between BO_6 octahedra. The ratio of cubic/hexagonal stacking of AO_3 layers, and thus the ratio of corner-sharing/face-sharing links in the BO_6 network, is a function of the tolerance factor.[3] The tolerance factor of phases can be adjusted by simple cation substitutions or by changes in the oxygen stoichiometry, as the introduction of oxygen vacancies leads to a reduction of the transition metals and a change in B−O bond length. The $BaMnO_{3-x}$ ($0 < x < 0.35$) structural series, for example, exhibits a series of structures as a function of composition from 2H-$BaMnO_{3.00}$ which exhibits 100% hexagonal stacking, through 15R, 8H, 6H, and 10H forms to 4H-$BaMnO_{2.65}$ which has 50% cubic, 50% hexagonal stacking.[4,5] It is therefore clear that the structure adopted by a phase is strongly coupled to the oxidation state of the transition metal within it. In the search for new electronic materials and phenomena this coupling can be restrictive preventing the synthesis of a large number of target phases with desired structure/oxidation state combinations.

One stratergy to overcome this restriction is the topotactic manipulation of the anion lattice. By utilizing the differing diffusion rates of the cations and anions within a complex oxide, reactions performed at low temperatures can deintercalate oxide ions from solid structures with no significant change to the topology of the metal cation lattice. In this way the coupling between the transition metal oxidation state and structural topology present at high temperature can be removed, allowing the preparation of a wide range of metastable materials with novel oxidation state/structure combinations.

* To whom correspondence should be addressed. E-mail: michael.hayward@chem.ox.ac.uk. Tel: +44 1865 272623. Fax: +44 1865 272690.

(1) Cooper, S. L.; Egami, T.; Goodenough, J. B.; Zhou, J.-S. *Localized to itinerant electronic transition in perovskite oxides*; Springer-Verlag: Berlin, 2001.
(2) Goldschmidt, V. M. *Naturwissenschaften* **1926**, *14*, 477.
(3) Darriet, J.; Subramanian, M. A. *J. Mater. Chem.* **1995**, *5*, 543.
(4) Negas, T.; Roth, R. S. *J. Solid State Chem.* **1971**, *3*, 323.
(5) Adkin, J. J.; Hayward, M. A. *Chem. Mater.* **2007**, *19*, 755.

10.1021/ic801185z CCC: $40.75
Published on Web 10/29/2008

A number of different reducing agents have been utilized to bring about these transformations. Taking examples based on manganese perovskite phases, hydrogen gas has been used to reduce $CaMnO_3$ topotactically to $CaMnO_{2.5}$[6] or $La_{0.5}Ca_{0.5}MnO_3$ and $La_{0.5}Sr_{0.5}MnO_3$ to the brownmillerite phases $La_{0.5}Ca_{0.5}MnO_{2.5}$ and $La_{0.5}Sr_{0.5}MnO_{2.5}$, respectively.[7,8] Additionally highly electropositive metals (Ti, Zr, Al, etc.) have been used as oxygen "getters" as in the preparation of $LaMnO_{2.8}$ via the reduction of $LaMnO_3$ with Zr.[9] However, both hydrogen and metal getters require relatively high reaction temperatures and appear to be limited to producing phases with a minimum manganese oxidation state of +2.5. Recently it has been demonstrated that binary metal hydrides can bring about the low temperature topotactic reduction of complex transition metal oxides.[10,11] Here we report the preparation of a new Mn(II) phase 4H-$Ba_{0.5}Sr_{0.5}MnO_{2+\delta}$ by the low temperature topotactic reduction of 4H-$Ba_{0.5}Sr_{0.5}MnO_{3-x}$.

Experimental Section

Preparation of Starting Materials. Five gram samples of 4H-$Ba_{0.5}Sr_{0.5}MnO_{3-x}$ were prepared by a ceramic route as described previously.[12] Suitable quantities of $BaCO_3$ (99.997%, Alfa Aesar), $SrCO_3$ (99.994%, Alfa Aesar), and MnO_2 (99.999%, Alfa Aesar) were thoroughly mixed in an agate pestle and mortar before being heated at 900 °C in air to decompose the carbonates. The resulting black powders were reground and pressed into 13 mm pellets under 5 tons pressure before being heated for two periods of 2 days at 1300 °C under flowing argon. Samples were reground and pressed into pellets between heating periods. After the final heating period, samples were cooled at 10 °C per minute to room temperature under argon. X-ray powder diffraction data collected from samples could be indexed on the basis of the hexagonal cell ($a = 5.585(1)$Å, $c = 9.212(1)$Å), consistent with previous reports.[12]

Reduction of 4H-$Ba_{0.5}Sr_{0.5}MnO_{3-x}$ Phases. Small (~300mg) samples of 4H-$Ba_{0.5}Sr_{0.5}MnO_{3-x}$ were mixed thoroughly with a four-fold stoichiometric quantity of LiH (Alfa Aesar 99.4%) or NaH (Aldrich 95%) in an argon filled glove box (O_2 and H_2O levels < 1ppm). These mixtures were then sealed under vacuum in Pyrex ampoules and heated at temperatures between 150 °C and 350 °C. Samples were subsequently washed with dry methanol under an inert atmosphere to remove lithium (LiH, Li_2O) and sodium (NaH, NaOH) containing phases, before being dried under vacuum.

Because of the hazards associated with the production of hydrogen gas when using lithium hydride as a reducing agent (described below) large samples suitable for neutron powder diffraction studies were prepared within a spring loaded "venting" apparatus to prevent the build up of gas pressure, as described previously.[13] 4:1 stoichiometric mixtures of LiH and 4H-$Ba_{0.5}Sr_{0.5}MnO_{3-x}$ were heated at 350 °C for two periods of 2 days with intermediate regrinding. Samples were then washed with dry methanol under an inert atmosphere to remove the lithium containing phases (LiH and Li_2O). Samples were then dried thoroughly by heating at 175°C for 6 h under flowing argon to remove any remaining solvent.

Characterization. X-ray powder diffraction data were collected from samples contained within home-made air sensitive sample holders using a Panalytical X'pert diffractometer incorporating an X'celerator position sensitive detector (monochromatic Cu $K_{\alpha 1}$ radiation). Neutron powder diffraction data were collected using the POLARIS instrument at the ISIS neutron source, Rutherford Appleton Laboratory, U.K. Data were collected from a sample contained in a vanadium can which had been sealed under argon with an indium washer in the case of the 1.8 K and 298 K data sets, or a copper gasket in the case of the 373 K data set. Rietveld structural refinements were performed against X-ray and neutron powder diffraction data using the GSAS suit of programs.[14] Thermogravimetric reoxidation measurements were performed on powder samples under flowing oxygen using a Netzsch STA 409PC balance. Average manganese oxidation states were also determined by dissolving samples in HCl containing an excess of KI and titrating the liberated I_2 with $Na_2S_2O_3$. Magnetization data were collected in the temperature range $5 < T/K < 400$ from powdered samples using a Quantum Design MPMS SQUID magnetometer.

Results

Chemical Reactivity of 4H-$Ba_{0.5}Sr_{0.5}MnO_{3-x}$. X-ray powder diffraction data collected from the products of the reaction between 4H-$Ba_{0.5}Sr_{0.5}MnO_{3-x}$ and LiH showed that at temperatures below 275 °C there was no significant reaction. At temperatures above 350 °C, reaction lead to decomposition of the quaternary oxide phase and the formation of simple binary oxides (MnO, SrO, BaO). In the temperature range $275 \leq T/°C \leq 350$ however, X-ray powder diffraction data collected from washed reaction products could be readily indexed on the basis a hexagonal unit cell ($a = 5.717(1)$Å, $c = 9.417(1)$).

Thermogravimetric reoxidation measurements (Figure 1) and iodometric titrations performed on samples of 4H-$Ba_{0.5}Sr_{0.5}MnO_{3-x}$ reduced with LiH gave overall stoichiometries of $Ba_{0.5}Sr_{0.5}MnO_{2.03(3)}$ and $Ba_{0.5}Sr_{0.5}MnO_{2.02(2)}$, respectively, consistent with the formulation $Ba_{0.5}Sr_{0.5}MnO_{2+\delta}$. The above observations are consistent with the simple topotactic reduction of 4H-$Ba_{0.5}Sr_{0.5}MnO_{3-x}$, suggesting reactions are proceeding according to scheme 1.

$$4\text{H-}Ba_{0.5}Sr_{0.5}MnO_{3-x} + 2y\,LiH \rightarrow 4\text{H-}Ba_{0.5}Sr_{0.5}MnO_{3-x-y} + y\,Li_2O + y\,H_2 \quad (1)$$

$$4\text{H-}Ba_{0.5}Sr_{0.5}MnO_{3-x} + y\,NaH \rightarrow 4\text{H-}Ba_{0.5}Sr_{0.5}MnO_{3-x-y} + y\,NaOH \quad (2)$$

This demonstrates that lithium hydride can act as a powerful solid state reducing agent at low temperatures in a

(6) Poeppelmeier, K. R.; Leonowicz, M. E.; Scanlon, J. C.; Longo, J. M.; Yelon, W. B. *J. Solid State Chem.* **1982**, *45*, 71.
(7) Gonzalez-Calbet, J. M.; Herrero, E.; Rangavittal, N.; Alonso, J. M.; Martinez, J. L.; Vallet-Regi, M. *J. Solid State Chem.* **1999**, *148*, 158.
(8) Cortes-Gil, R.; Ruiz-Gonzalez, M. L.; Alonso, J. M.; Vallet-Regi, M.; Hernando, M.; Gonzalez Calbet, J. M. *Chem.—Eur. J.* **2007**, *13*, 4246.
(9) Hansteen, O. H.; Breard, Y.; Fjellvag, H.; Hauback, B. C. *Solid State Sci.* **2004**, *6*, 279.
(10) Hayward, M. A.; Green, M. A.; Rosseinsky, M. J.; Sloan, J. *J. Am. Chem. Soc.* **1999**, *121*, 8843.
(11) Hayward, M. A.; Cussen, E. J.; Claridge, J. B.; Bieringer, M.; Rosseinsky, M. J.; Kiely, C. J.; Blundell, S. J.; Marshall, I. M.; Pratt, F. L. *Science* **2002**, *295*, 1882.
(12) Adkin, J. J.; Hayward, M. A. *J. Solid State Chem.* **2006**, *179*, 70.
(13) O'Malley, M.; Lockett, M. A.; Hayward, M. A. *J. Solid State Chem.* **2007**, *180*, 2851–2858.
(14) Larson, A. C.; Von Dreele, R. B. *General Structure Analysis System*; Los Alamos National Laboratory Report LAUR 86-748; Los Alamos National Laboratory: Los Alamos, NM, 2000.

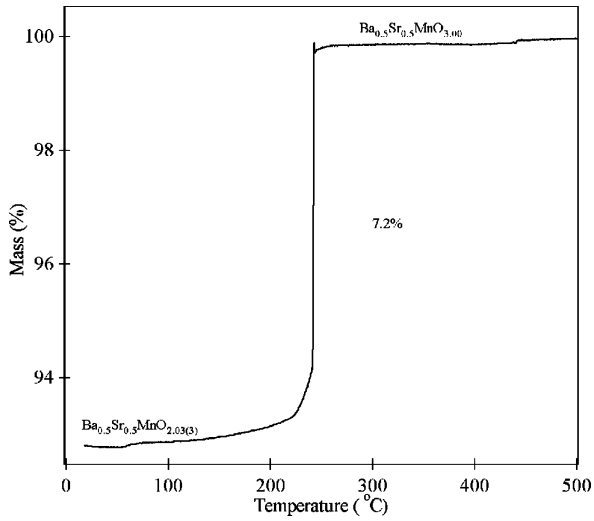

Figure 1. Thermogravimetric data collected during the oxidation of $Ba_{0.5}Sr_{0.5}MnO_{2.03(3)}$ to $Ba_{0.5}Sr_{0.5}MnO_{3.00}$.

manner analogous to sodium hydride or calcium hydride.[10,11] The formation of lithium oxide (confirmed by X-ray powder diffraction) and hydrogen gas as reaction products indicates that the hydride ion in this case acts as a single electron reducing agent.

Similar reduction reactions were observed between 4H-$Ba_{0.5}Sr_{0.5}MnO_{3-x}$ and sodium hydride in the temperature range $150 \leq T/°C \leq 225$ consistent with reaction scheme 2. However, when the sample reduced with sodium hydride was washed with methanol under an inert atmosphere, to remove NaOH and any remaining NaH, the sample decomposed/dissolved. Washing the sample reduced with lithium hydride lead to no observable change in the X-ray powder diffraction patterns of the 4H-$Ba_{0.5}Sr_{0.5}MnO_{2+\delta}$ phase; therefore, large samples suitable for detailed characterization were prepared using lithium hydride as a reducing agent as described above.

Characterization of 4H-$Ba_{0.5}Sr_{0.5}MnO_{2+\delta}$. Zero-field cooled and field-cooled magnetization data were collected from 4H-$Ba_{0.5}Sr_{0.5}MnO_{2+\delta}$ in an applied field of 1000 Oe in the temperature range $5 < T/K < 400$ as shown in Figure 2a. The zero-field cooled data in the range $5 < T/K < 290$ can be fitted to a Curie−Weiss + TIP relation ($M/H = C/(T - \theta) + K$) as shown in Figure 2b. The very low Curie constant extracted ($C = 0.0685(6)$ cm^3 K mol^{-1}) is consistent with a small quantity (2.2 mol %) of Mn(III) $s = 2$ centers, suggesting this signal is due to the presence of a small number of Mn(III) impurity centers with the bulk of the sample not contributing to the temperature dependent part of the magnetization. The lack of any contribution to the magnetization from the Mn(II) centers present in the material and the divergence between zero field-cooled and field-cooled data at $T \sim 355$ K (Figure 2a) suggests the onset of canted antiferromagnetic order at this temperature.

Neutron powder diffraction data collected from 4H-$Ba_{0.5}Sr_{0.5}MnO_{2+\delta}$ at 373 K could be readily indexed using the unit cell refined from the X-ray powder diffraction data ($a = 5.717(1)$Å, $c = 9.417(1)$) and were consistent with the $P6_3/mmc$ space group. A structural model based on that of 4H-$Ba_{0.5}Sr_{0.5}MnO_{2.79}$[12] was refined against these data. The

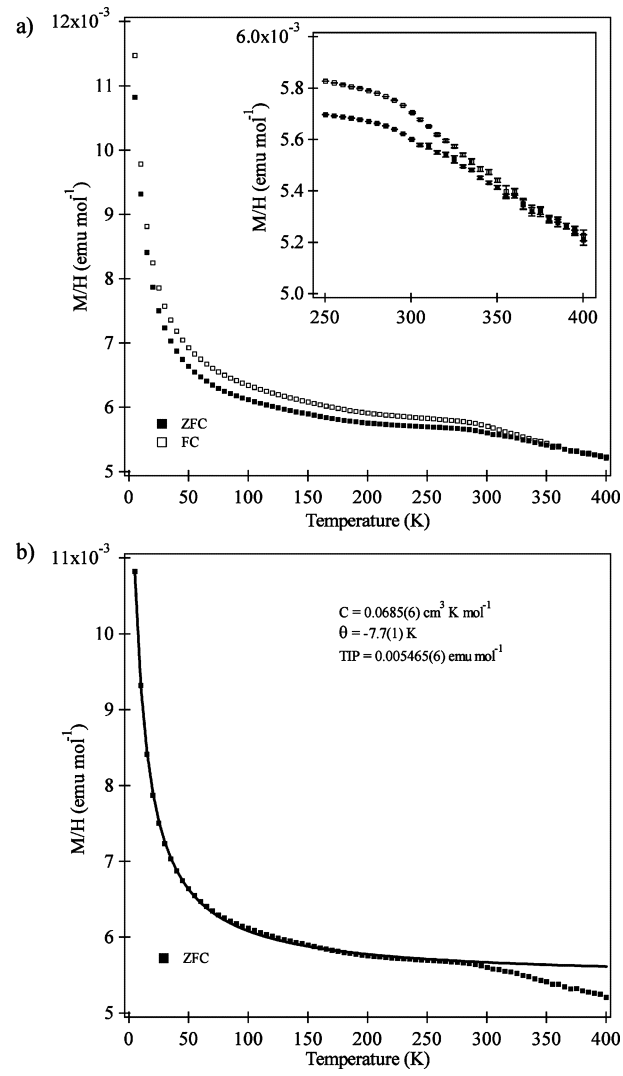

Figure 2. (a) Zero-field cooled and field-cooled magnetization data collected from $Ba_{0.5}Sr_{0.5}MnO_{2+\delta}$. Inset shows data converge at ~355 K. (b) Curie−Weiss + TIP fit to zero-field cooled data.

atomic positions and anisotropic displacement factors of all atoms were refined along with the oxide ion occupancy numbers. Particular attention was paid to the occupancies of the two oxide ion sites, as these were strongly correlated with the associated displacement ellipsoids. To remove this correlation, the oxide ion occupancies were constrained such that the overall refined composition was consistent with that obtained chemically. The large displacement parameters refined for the anion sites were suggestive of static disorder. To test this, models in which the anion scattering was split between a number of lower symmetry sites were constructed. However these structural models were unstable and would not converge, so the high symmetry description was retained. The barium and strontium occupancy numbers were not refined but were set to the values obtained from the room temperature structural refinement of 4H-$Ba_{0.5}Sr_{0.5}MnO_{2.79}$ in which there is partial Ba/Sr ordering driven by the different sizes of the two A-cation sites.[12] Close inspection of the fit to the data revealed a number of weak reflections corresponding to a small quantity (1.8(1) mol %) of MnO in the

Table 1. Structural Parameters Refined against Neutron Powder Diffraction Data Collected from 4H-$Ba_{0.5}Sr_{0.5}MnO_{2+\delta}$ at 1.8, 298, and 373 K

			temperature		
atom	position	variable	1.8 K	298 K	373 K
Ba/Sr1	2a (0,0,0)	fractional occupancy	0.67/0.33		
		U_{equiv} (Å^3)	0.0522	0.0728	0.0788
Ba/Sr2	2c ($^1/_3$,$^2/_3$,$^1/_4$)	fractional occupancy	0.33/0.67		
		U_{equiv} (Å^3)	0.0428	0.0512	0.0553
Mn	4f ($^1/_3$,$^2/_3$,z)	z	0.6069(4)	0.6069(3)	0.6070(3)
		U_{equiv} (Å^3)	0.0123	0.0140	0.0165
		ordered moment (μ_B)	3.73(3)	1.92(3)	0
O1	6g ($^1/_2$,0,0)	fractional occupancy	0.813(6)		
		U_{equiv} (Å^3)	0.1383	0.1411	0.1479
O2	6h (x,2x,$^1/_4$)	x	−0.1770(5)	−0.1795(4)	−0.1778(4)
		fractional occupancy	0.534(6)		
		U_{equiv} (Å^3)	0.0724	0.0789	0.0784
a (Å)			5.7005(3)	5.7179(6)	5.720(2)
c (Å)			9.3776(5)	9.4179(9)	9.429(4)
χ^2			2.206	3.256	2.075
wRp			1.54%	1.88%	1.19%
Rp			1.71%	2.17%	1.71%

Table 2. Selected Bond Lengths and Angles Extracted from the Refined Structure of 4H-$Ba_{0.5}Sr_{0.5}MnO_{2+\delta}$ and 4H-$Ba_{0.5}Sr_{0.5}MnO_{2.79}$ from Reference 12

	bond length(Å)/angle(deg)	
bond	4H-$Ba_{0.5}Sr_{0.5}MnO_{2+\delta}$	4H-$Ba_{0.5}Sr_{0.5}MnO_{2.79}$
Ba/Sr1−O1	2.8590(3)	2.793(1)
Ba/Sr1−O2	2.950(2)	2.923(1)
Ba/Sr2−O1	2.8754(5)	2.811(1)
Ba/Sr2−O2	2.8618(3)	2.799(1)
Mn1−O1	1.933(4)	1.900(1)
Mn1−O2	2.034(3)	1.927(2)
Mn2−Mn2	2.696(5)	2.596(3)
Mn2−O2−Mn2	78.24(7)	84.69(1)

sample. MnO was therefore added to the structural model as a second phase. The refinement converged readily. Details of the refined structural model are shown in Table 1, with details of the anisotropic displacement parameters of all atoms listed in the Supplementary Information. Selected bond lengths are listed in Table 2. A comparison of the observed and calculated diffraction patterns is shown in Figure 3a, with a depiction of the overall structure shown in Figure 4a.

Neutron powder diffraction data collected from 4H-$Ba_{0.5}Sr_{0.5}MnO_{2+\delta}$ at 298 K and 2 K show significant changes to the intensity of diffraction features at large d-spacing (Figure 3). As noted above, the transition observed at 355 K in the magnetic susceptibility of 4H-$Ba_{0.5}Sr_{0.5}MnO_{2+\delta}$ (Figure 2) suggests that this additional intensity is magnetic in origin. A magnetic model based on that of 4H-$Ba_{0.5}Sr_{0.5}MnO_{3.00}$[12] was therefore added to the structural model and refined against the two lower temperature data sets. This was found to account for the additional intensity well. Full details of the nuclear and magnetic models refined from the data collected at 298 K and 1.8 K are listed in Table 1. A comparison of the observed and calculated diffraction patterns shown in Figure 3, with the relative orientations of the magnetic moments refined from the low temperature neutron diffraction data shown in Figure 4b.

Discussion

The topotactic reduction of 4H-$Ba_{0.5}Sr_{0.5}MnO_{3-x}$ with LiH to form 4H-$Ba_{0.5}Sr_{0.5}MnO_{2+\delta}$ leads to an increase in all the lattice parameters and metal−oxygen bond lengths as shown in Tables 1 and 2. This expansion is consistent with the expected increase in the ionic radius of manganese on reduction from a mean oxidation state of +3.58 to +2.01. An analogous expansion is observed on the reduction of 4H-

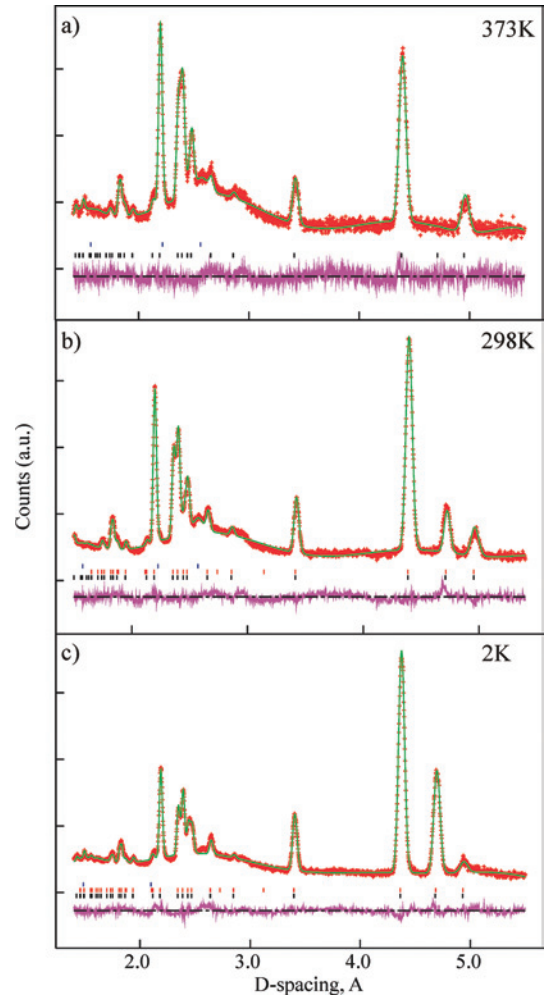

Figure 3. Observed, calculated, and difference plots from the structural refinement of 4H-$Ba_{0.5}Sr_{0.5}MnO_{2+\delta}$ against neutron powder diffraction data collected from the 35° bank of the POLARIS diffractometer. (a) Refinement of a nuclear only model against data collected at 373 K; combined nuclear and magnetic models refined against data collected at (b) 298 K and (c) 2 K. All structural models include contributions from a minority (1.56 mol %) MnO impurity phase.

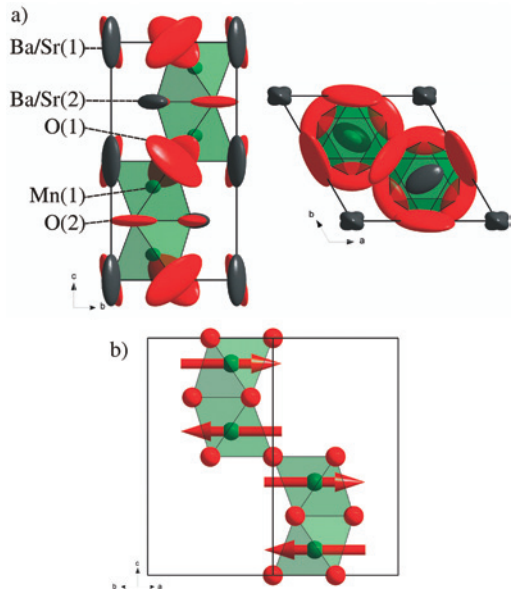

Figure 4. (a) Structure of $Ba_{0.5}Sr_{0.5}MnO_{2+\delta}$ refined from neutron data collected at 373 K. (b) A representation of the relative spin orientations in the antiferromagnetic model refined against neutron powder diffraction data collected at 1.8 K.

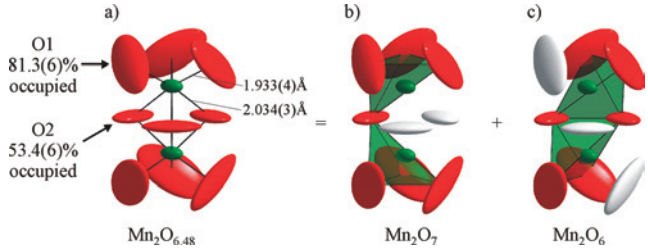

Figure 5. $Mn_2O_{6.48}$ structural unit (a) considered as the superposition of (b) Mn_2O_7 and (c) Mn_2O_6 units which are in turn constructed from pairs of corner and edge linked MnO_4 tetrahedra, respectively.

$Ba_{0.5}Sr_{0.5}MnO_{3.00}$ to 4H-$Ba_{0.5}Sr_{0.5}MnO_{2.79}$.[12] The refined structure of 4H-$Ba_{0.5}Sr_{0.5}MnO_{2+\delta}$ reveals that the oxide ions vacancies are located primarily in anion sites which connect the MnO_6 octahedra of 4H-$Ba_{0.5}Sr_{0.5}MnO_{3-x}$ in a face-sharing manner (O2). In addition there are also a significant number of vacancies on the O1 anion site which connect the MnO_6 units in a corner-sharing manner. The preference for locating vacancies on the O2 site can be rationalized using arguments based on the Ba/Sr−O bond lengths of the two anion sites employed previously to explain the anion vacancy distribution in the 4H-$Ba_{0.5}Sr_{0.5}MnO_{3-x}$ parent phase.[12]

If we consider the different manganese coordination environments present in the structure, we can see that the Mn_2O_9 dimer units present in ideal 4H-$Ba_{0.5}Sr_{0.5}MnO_{3.00}$ adopt an average composition of $Mn_2O_{6.48}$ on reduction (Figure 5a). These $Mn_2O_{6.48}$ units can be considered as the superposition of Mn_2O_7 and Mn_2O_6 units as shown in Figure 5. The Mn_2O_7 unit shown in Figure 5b consisting of a pair of corner sharing MnO_4 "tetrahedra" formed by the removal of two oxide ions from O2 sites is analogous to iron coordination sites seen in the anion deficient hexagonal perovskites $BaFeO_{2.8}$ and $BaMn_{0.4}Fe_{0.6}O_{2.73}$.[15,16] The Mn_2O_6 unit is slightly more complex as it can be formed by either removing an oxide ion from an O1 site and an O2 site disposed in a *cis* manner to form a pair of edge sharing "tetrahedra" (Figure 5c) or a pair of edge sharing square planes can be produced, if the two oxide ions removed from the MnO_6 octahedron have a *trans* relationship. Similar arrays of edge sharing square-planar units have been observed previously in another anion deficient hexagonal perovskite $BaNiO_2$.[17] However, while square planar coordinations are common for Ni(II) they are almost unprecedented for manganese. We therefore think this coordination is rather unlikely and so will not consider this structural configuration further and assume all the Mn_2O_6 units exist as pairs of edge sharing tetrahedra.

Inspection of the Mn−O bond lengths in the refined structure of 4H-$Ba_{0.5}Sr_{0.5}MnO_{2+\delta}$ (Figure 5a) shows that the manganese ions are displaced away from the shared face of the Mn_2O_{9-x} unit increasing the Mn−Mn separation relative to that observed in 4H-$Ba_{0.5}Sr_{0.5}MnO_{2.79}$ (Table 2). This is consistent with an increase in the Mn−Mn coulombic repulsion on the removal of anions from the O2 site. The two tetrahedral MnO_4 coordinations present in the refined structure 4H-$Ba_{0.5}Sr_{0.5}MnO_{2+\delta}$ have bond lengths (average Mn−O = 1.958Å and 1.983Å, Table 2) which are broadly comparable to other Mn(II)O_4 tetrahedra such as those in Mn_3O_4 (Mn−O = 2.078Å[18]) or the topotactically reduced phases $Sr_7Mn_4O_{12}$ (average Mn−O = 1.978Å[19]) and $La_{.75}Sr_{0.25}MnO_{2.5}$ (average Mn−O = 2.032Å[20]). The displacement parameters refined for the anion sites in 4H-$Ba_{0.5}Sr_{0.5}MnO_{2+\delta}$ are very large and do not diminish with decreasing temperature (Table 1). This behavior suggests the displacement ellipsoids are modeling a static disordered displacement of the anions in this phase. Such displacements can arise from the disordered twisting of the MnO_4 units in the structure to accommodate the increase in Mn−O bond lengths on reduction. As noted above attempts to model the scattering with a disordered displacement model failed. It should be noted, however, that the observation of large displacement parameters for the anions in this phase makes it likely that the metal oxygen bond lengths quoted in Table 2 underestimate the true values. Similar large displacement ellipsoids have been observed for other reduced manganates ($YSr_2Mn_2O_{7-x}$ and $Sr_4Mn_{2.88}O_{7.04}Cu_2S_2$[21,22]) and appear to be a common structural feature of these phases.

The ordered moment refined from the data collected at 1.8 K (3.73(3) μ_B) is ∼75% of the value expected for an *s*

(15) Delattre, J. L.; Stacy, A. M.; Siegrist, T. *J. Solid State Chem.* **2004**, *117*, 928–935.
(16) Miranda, L.; Boulahya, K.; Varela, A.; Gonzalez Calbet, J. M.; Parras, M.; Hernando, M.; Fernandez-Diaz, M. T.; Feteira, A.; Sinclair, D. C. *Chem. Mater.* **2007**, *19*, 3425–3432.
(17) Lander, J. J. *Acta Crystallogr.* **1951**, *4*, 148–156.
(18) Satomi, K. *J. Phys. Soc. Jpn.* **1961**, *16*, 258–265.
(19) Hayward, M. A. *Chem. Commun.* **2004**, 170.
(20) Casey, P. S.; Barker, D.; Hayward, M. A. *J. Solid State Chem.* **2006**, *179*, 1375.
(21) Hayward, M. A. *Chem. Mater.* **2006**, *18*, 321.
(22) Hyett, G.; Barrier, N.; Clarke, S. J.; Hadermann, J. *J. Am. Chem. Soc.* **2007**, *129*, 11192–11201.

$= {}^5/_2$ center. This relatively low value is presumably due in part to the structural disorder present in the material. The high magnetic ordering temperature observed for 4H-$Ba_{0.5}Sr_{0.5}MnO_{2+\delta}$ (355K) is not unexpected for a number of reasons. First, all members of the $BaMnO_{3-x}$ hexagonal perovskite series (with the exception of 2H-$BaMnO_3$), on which 4H-$Ba_{0.5}Sr_{0.5}MnO_{2+\delta}$ is based, exhibit strong magnetic coupling.[5] $Ba_{0.5}Sr_{0.5}MnO_{3.00}$ exhibits antiferromagnetic order below 260 K, but $Ba_{0.5}Sr_{0.5}MnO_{2.79}$ undergoes a transition to a magnetically glassy phase at $T \sim 150$K because of Mn(III)/Mn(IV) charge disorder.[12] Second, the presence of an extended network of Mn(II) centers would be expected to exhibit strong magnetic coupling because of the large moment this d^5 $s = {}^5/_2$ ion possesses. Complex oxides containing d^5 centers such as Fe(III) commonly have high magnetic ordering temperatures as exemplified by the Ln-FeO_3 (Ln = lanthanide) series of perovskites ($620 < T_N/K < 740$[23]). However, in contrast to Fe(III) containing phases there are few magnetically ordered Mn(II) containing oxides with which to compare the magnetic behavior of $Ba_{0.5}Sr_{0.5}MnO_{2+\delta}$. This is because although there are a large number of Mn(II) containing oxides, the manganese centers in these materials tend to be isolated from each other (as observed in Sr_2MnWO_6 and $Ba_3MnMn_2O_9$ for example[24,25]) rather than forming an extended Mn−O−Mn network. This large spatial separation between manganese centers limits the strength of any magnetic coupling.

There are some suitable materials for comparison, most notably $YSr_2Mn_2O_{5.5}$, the Mn(II) product of the topotactic reduction of $YSr_2Mn_2O_7$.[21] Magnetic susceptibility measurements and neutron diffraction data collected from this phase at 300 K provide evidence for short range magnetic order at this temperature, which becomes fully three-dimensional and long range on cooling. Presumably the large distortion observed in the structure of $YSr_2Mn_2O_{5.5}$ weakens the magnetic coupling between manganese centers leading to short range behavior at high temperature. In contrast the long range three-dimensional antiferromagnetic order observed in 4H-$Ba_{0.5}Sr_{0.5}MnO_{2+\delta}$ demonstrates that despite the significant disordered structural distortion observed in this phase (as indicated by the large oxide ion displacement parameters) strong magnetic coupling is retained. This suggests that other Mn(II) phases with extended Mn−O−Mn networks should also exhibit strong magnetic coupling and high magnetic ordering temperatures.

Acknowledgment. We thank R. Smith for assistance collecting neutron powder diffraction data and the EPSRC for funding this work.

Supporting Information Available: Complete description of the displacement ellipsoids refined for 4H-$Ba_{0.5}Sr_{0.5}MnO_{2+\delta}$. This material is available free of charge via the Internet at http://pubs.acs.org.

IC801185Z

(23) Goodenough, J. B.; Longo, J. M. *Landolt-Börnstein Tabellen*; Springer: Berlin, 1970; p 228.
(24) Munoz, A.; Alonso, J. A.; Casais, M. T.; Martinez-Lope, M. J.; Fernandez-Diaz, M. T. *J. Phys.:Condens. Matter* **2002**, *14*, 8817.
(25) Lui, Y.; Withers, R. L.; Wichello, A. P.; Noren, L.; Ting, V.; Brink, F.; Gerald, J. D. F. *J. Solid State Chem.* **2005**, *178*, 3389–3395.